ChemBioChem

Research Article
doi.org/10.1002/cbic.202400727

Chemistry Europe
European Chemical Societies Publishing

www.chembiochem.org

Mechanisms in the Synthesis of *S*-Alcohols with 1,4-NADH Biomimetic Co-factor N-Benzyl-1,4-dihydronicotinamide using Horse Liver Alcohol Dehydrogenase: A Hybrid Computational Study

Matteo Farina,[a] Matteo Capone,[b] Enrico Bodo,[a] Richard H. Fish,*[c] Massiliano Aschi,[b] Alessandro Marrone,*[d] and Isabella Daidone*[b]

The enantioselective reduction of prochiral ketones catalyzed by horse liver alcohol dehydrogenase (HLADH), was investigated via a hybrid computational approach, for molecular reactions involved in chiral synthesis of *S*-alcohols, when the natural co-factor, 1,4-dihyronicotinamide adenine dinucleotide, 1,4-NADH, was replaced with biomimetic co-factor, N-benzyl-1,4-dihydronicotinamide, **1**. We surmised that different hydride and proton transfer mechanisms were involved using co-factor, **1**. An alternative mechanism, where the hydride transfer step occurred, via an η^1-keto-*S*-η^2-5,6-1,4-dihydronicotinamide-Zn(II) complex, was previously investigated with a model of the HLADH–Zn(II) catalytic site (*J. Organometal. Chem.* **2021**, *943*, 121810). Presently, we studied canonical and alternative mechanisms compared to models of the entire enzyme structure. We disproved the η^2-Zn(II) complex, and discovered a canonical hydride transfer from biomimetic 1,4-NADH, **1**, to the Zn(II) bound prochiral ketone substrate, followed by a new proton relay, consisting of a water chain connecting His51 to Ser48 that accomplished the *S*-alkoxy anion's protonation to yield the final *S*-alcohol product. The HLADH catalysis, with biomimetic co-factor, **1**, that replaced the ribose group, the 5′-diphosphate groups, and the adenine nucleotide with a N-benzyl group, has provided a new paradigm for the design of other structures of 1,4-NADH biomimetic co-factors, including their economic value in biocatalysis reactions.

Introduction

The biocatalysis discipline has been shown to be an outstanding technique for the synthesis of chiral organic chemicals.[1–3] The deployment of enzymes in organic synthesis have been shown to be exceedingly attractive, due to the higher yields of chiral products,[4–6] in terms of chemo and stereoselectivity, and their ability to operate under mild conditions, in aqueous solution.[7] More recently, there have been numerous studies on the methods to increase biocatalytic improvements, via the utilization of directed evolution methodology.[8–11] Among the available biocatalysts, the oxidoreductase enzymes have deserved special attention, since performing a chemical process that was particularly challenging, or not possible in an aqueous environment, utilizing non-enzymatic conditions; for example, alkane hydroxylation, aromatic ring functionalization, or hydride transfer reactions.[12] Therefore, a vast body of data and information has been accumulated concerning the employment of oxidoreductases enzymes in chiral chemical synthesis, while the horse liver alcohol dehydrogenase enzyme (HLADH) has been extensively studied for this purpose.[13–15] In the most accredited HLADH mechanistic hypothesis,[14,16,17] the reactive ternary adduct (Scheme 1) was formed by the η^1-O-coordination of the ketone carbonyl substrate to the Zn(II) center, and by the approach of the 1,4-NADH co-factor, via several non-covalent interactions, which stabilized the co-factor in the active position, thus allowing the proximity of its C4–H bond to the ketone substrate carbonyl group. The subsequent hydride transfer (**HT**) step yielded the configuration, in which the Zn(II) coordinated ketone substrate was converted into the corresponding *S*-alkoxy anion, while forming the NAD^+ co-factor. In subsequent steps, conversion to the chiral *S*-alcohol occurred by a proton relay system that transfers a proton from the bulk to the oxygen of the Zn(II) bound *S*-alkoxy anion. The Zn(II) bound *S*-alkoxy anion then undergoes the final protonation reaction, with the release of the chiral *S*-alcohol and NAD^+ (Scheme 1).

[a] *M. Farina, E. Bodo*
Dipartimento di Chimica, Università degli Studi di Roma La Sapienza, Roma, IT

[b] *M. Capone, M. Aschi, I. Daidone*
Dipartimento di Scienze Fisiche e Chimiche, Università degli Studi dell'Aquila, L'Aquila, IT
E-mail: isabella.daidone@univaq.it

[c] *R. H. Fish*
Lawrence Berkeley National Laboratory, University of California, Berkeley, CA 94720, USA
E-mail: rhfish@lbl.gov

[d] *A. Marrone*
Dipartimento di Farmacia, Università degli Studi G. d'Annunzio, Chieti-Pescara, IT
E-mail: amarrone@unich.it

Supporting information for this article is available on the WWW under https://doi.org/10.1002/cbic.202400727

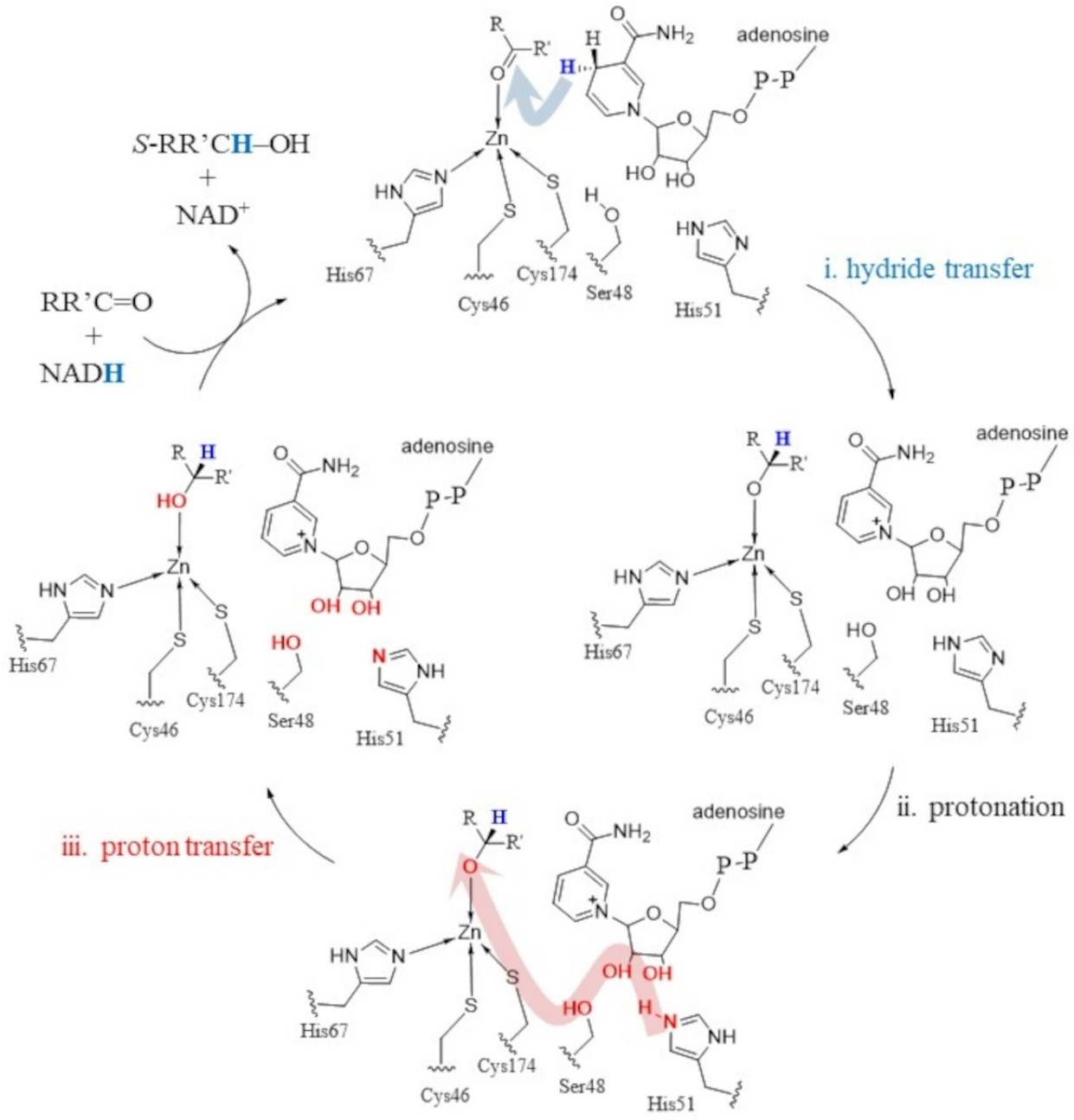

Scheme 1. The mechanism of the HLADH catalyzed reduction of a prochiral ketone substrate in the presence of the natural 1,4-NADH co-factor. The atoms involved in the proton relay, and the hydride transfer, are colored (**red**) and (**blue**), respectively.[16]

One of the paradigms in Scheme 1 describing the HLADH enzymatic mechanism was the non-covalent binding between the natural 1,4-NADH co-factor and the protein.[14,16,17] In the canonical structure, the binding of the natural 1,4-NADH co-factor at the HLADH pocket relied on numerous weak interactions, predominantly along the extended N-1,4-dihydronicotinamide nucleotide-5′-diphosphate adenine nucleotide structure, which was found to be particularly high in potential hydrogen bonding functionalities. Thus, with the accommodation of this polar group, the 1,4-dihydronicotinamide structure was conformationally situated in the proximity of the Zn(II) bound ketone substrate's carbonyl group. Several authors have proposed that the key step of the HLADH reductive pathway, the donation of the 1,4-NADH hydride to the carbonyl carbon of the prochiral ketone substrate, was determined by the fact that one C4–H bond on the 1,4-dihydronicotinamide structure was at the favorable distance, and at the orientation to favor the hydride transfer, via the tunneling effect.[16,17]

The importance of the HLADH enzyme, involved in the non-covalent interactions with 1,4-NADH, has been well documented by a number of publications, and thus, even if the 1,4 dihydronicotinamide ring was the chemically active structure,

the adenine dinucleotide pendant played a relevant role in the HLADH catalysis.[14,15] More importantly, several studies have ascertained that the HLADH biomimetic co-factors, whose structure contained no adenine dinucleotide groups, but instead, had an organic group at the N1 position, and was an efficient substitute for the natural 1, 4 NADH co-factor.[18–25] Furthermore, the N-benzyl-1,4-dihydronicotinamide biomimetic co-factor, **1**, was probably the most extensively investigated 1,4-NADH biomimetic, due to the relatively high efficiency, and low cost (Figure 1).[19,23,24a]

In comparison to the natural 1,4-NADH co-factor, the biomimetic co-factor 1,4-NADH, **1**, was expected to interact differently with the HLADH catalytic site, since the important structural differences between the N-benzyl group and that of the ribose-diphosphate-adenine nucleotide groups. Alternatively, the biomimetic 1,4-NADH co-factor, **1**, and the other tested biomimetic co-factors, were found to provide the HLADH enzyme yields comparable to those obtained with the use of the natural 1,4-NADH co-factor, including *S*-enantioselectivity.[24a–b,25] The data further suggested that the 1,4-NADH biomimetic co-factor might be able to position the 1,4-dihydronicotinamide group in proximity to the prochiral ketone carbonyl group, providing the hydride transfer by either alternative sites in comparison to the natural co-factor.

To our knowledge, few structural descriptions concerning the binding of the 1,4-NADH biomimetic co-factors to the HLADH enzyme have been reported,[25] while the detailed structural studies on the binding of these biomimetic co-factors at the HLADH enzyme were found lacking. Another aspect connected to the significant structural differences between the biomimetic 1,4-NADH, co-factor, **1**, and the natural 1,4-NADH co-factor was represented by the Brønsted catalysis; the protonation of the Zn (II) bound *S*-alkoxy group, which represented the final step of the HLADH reduction catalysis to provide the chiral *S*-alcohol.

As proposed by several authors, this step was prompted by the participation of the ribose-OH groups, to a hydrogen bond pattern connecting the donor Ser48 residue to the Zn(II)-bound alkoxy oxygen. Thus, this proton relay accomplished the proton transfer (**PT**), after the hydride transfer step (Scheme 1); however, we demonstrated that this pattern cannot be formed when the biomimetic co-factor, **1**, or other biomimetic co-factors were used in place of the natural 1,4-NADH. Thus, the final protonation step must be accomplished through an alternative mechanism.

The above highlighted occurrences pointed to several critical aspects about the current paradigm for the HLADH catalytic mechanism, when the reductive pathway to form the chiral *S*-alcohol product was considered. Recently, an alternative reductive route to the HLADH catalysis has been proposed based on the Density Functional Theory (DFT) calculations of the thermodynamics and kinetics of the enantioselective reduction of two ketone substrates; 2-pentanone and 4-phenyl-2-butanone, operating with the core model of the HLADH enzyme, including the biomimetic co-factor, **1**, while lacking the proteins surrounding the HLADH site of activity.[13,26]

Our previous calculations have shown that upon decomplexation of the 4-methylimidazole ligand from the Zn(II) metal center, the biomimetic co-factor, **1**, could possibly coordinate to the Zn(II) center by forming the η^2-5,6-N-benzyl-1,4-dihydronicotinamide-Zn(II) complex, with the natural HLADH enzyme.[26] By investigating the calculated structure of the η^2-intermediate, we had detected a close proximity between the C4–H bond of the biomimetic 1,4-NADH, **1**, with the ketone carbonyl group that facilitated the hydride transfer, via a very low activation energy.[26] Therefore, our calculations have clearly shown that the higher contribution to the kinetic barrier for the overall ketone to the alkoxy anion reaction was associated with the 4-methylimidazole decomplexation. Such a barrier has been previously quantified at 15 kcal/mol.[26]

Results and Discussion

A New HLADH Enzyme Mechanistic Paradigm

In the light of these previous computational results, and by taking into account the above highlighted critical points, we previously performed a computational investigation based on the combination of classical and quantum methods detailing

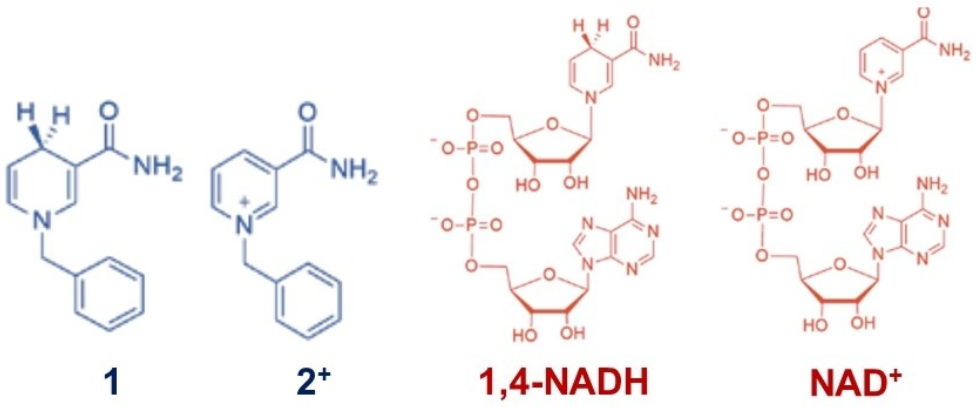

Figure 1. Structures of Biomimetic Co-factors, **1** and **2**$^+$; Natural Co-factor**s, 1,4-NADH** and **NAD**$^+$.

the structure of the HLADH active complex formed by the biomimetic co-factor, **1**; however, in the presence of the core amino acids surrounding the Zn(II) center, but in the absence of the proteins surrounding the HLADH site of reactivity. This approach was utilized to corroborate the viability of the newly proposed HLADH reductive route, based on the η^2-coordination of the N-benzyl-1,4 dihydronicotinamide's 5,6-carbon-carbon double bond to the Zn(II) metal ion center (Scheme 2).

In this computational study, the enantioselective reduction of the 2-pentanone catalyzed by HLADH in the presence of the biomimetic co-factor, N-benzy-l,4-dihydronicotinamide, **1**, was investigated by means of a multiscale computational approach based on the Perturbed Matrix Method (PMM),[27,28] to examine the possible viability of the mechanistic hypothesis proposed by Marrone and Fish,[26] and to define the most plausible mechanisms for both the hydride and proton transfer steps. Compared to the canonical mechanism (Scheme 1), the alternative mechanism proposed by Marrone and Fish[26] (Scheme 2) observed the hydride transfer from the C4–H of the biomimetic co-factor, **1**, to the prochiral ketone substrate, 2-pentanone, which occurred in two consecutive steps: (*1*) decomplexation of the His imidazole ligand yielding the 5,6-η^2-coordination of **1** to the catalytic Zn(II) metal ion center, and (*2*) the hydride transfer providing the Zn(II)-bound *S*-2-pentoxy anion, and the oxidized co-factor, the N-benzylnicotinamide cation, $\mathbf{2}^+$.

Although the canonical and alternative mechanisms were distinguishable based on the hydride transfer process, and the protonation of the *S*-2-pentoxy anion, bound to Zn (II), both these scenarios must be necessarily operating, via the relay of one proton from the bulk to the catalytic site of reactivity. Moreover, we firmly believed that a proton was an essential reactant in the total enzymatic process. In a resemblance to the HLADH catalysis occurring in the presence of the natural 1,4-NADH co-factor, we assumed that the His51 residue played a pivotal role in the proton relay, as well as when the enzyme catalysis took place in the presence of the biomimetic co-factor, **1**. Thus, the ionization state of the His51, with the side chain imidazole, either mono or doubly protonated, was employed to either turn *on* or *off*, the proton relay system.

This approach allowed us to model two pathways of the HLADH catalysis; in one pathway, we assumed that the proton relay was *off* in the HLADH resting state, thus leading to the hydride transfer and the *S*-2-pentoxy protonation occurring in two consecutive steps. Alternatively, we also assumed that the proton relay was occurring during the HLADH resting state, thus allowing the hydride and the proton transfers to be synchronous.

For major clarity, we utilized the word *mechanism* with reference to the type of operating hydride transfer, either canonical or alternative, and the word *pathway* with reference to the type of hydride and proton transfer steps, either nonsynchronous with HT or PT, in two consecutive steps, or with HT + PT in one synchronous step. The latter pathway required that the proton relay was *on* from the resting state, which meant that the His51 was doubly protonated in the initial HLADH configuration. Therefore, we also assumed the possible participation of water molecules, in the proton transfer steps, via the H-bond bridging between the protonated His and the Ser ligands. The mechanisms and pathways of the HLADH

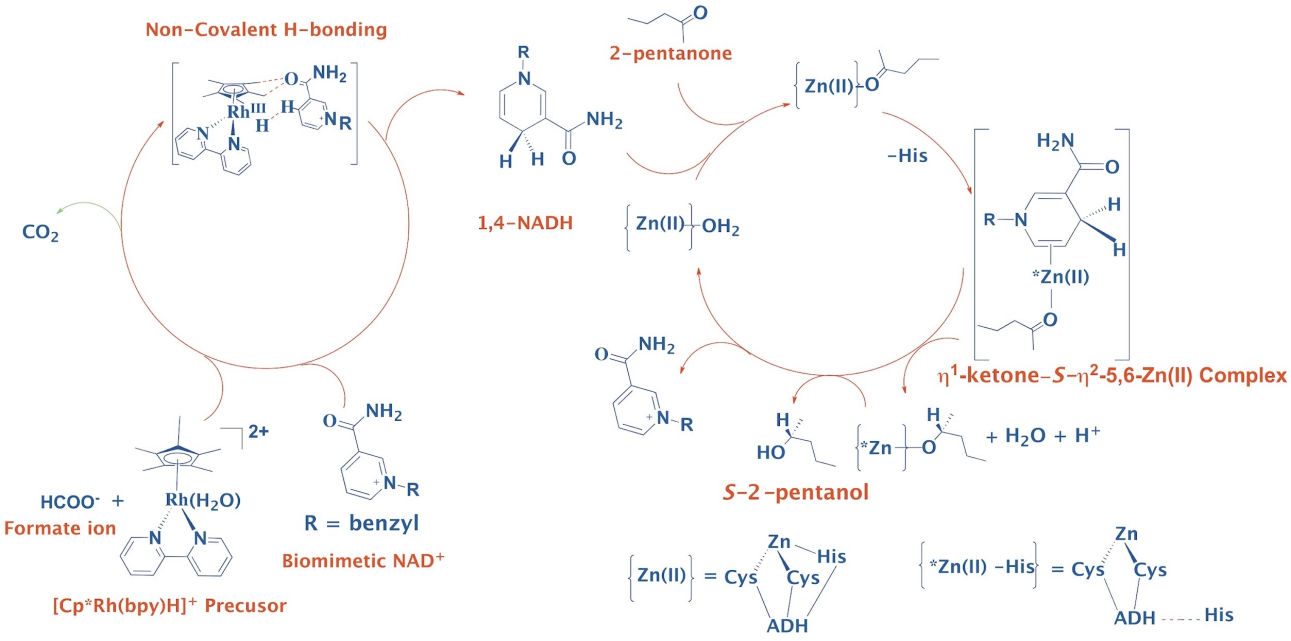

Scheme 2. The alternative mechanistic hypothesis proposed by Marrone and Fish[26] for the HLADH catalyzed chiral reduction of prochiral ketones in the presence of the 1,4-NADH biomimetic co-factor, **1**, obtained by using a core model of the HLADH catalytic site. The left side shows the first tandem catalysis component, the reduction of the biomimetic NAD^+ co-factor, $\mathbf{2}^+$, with the *in situ* generated reducing agent using the formate anion, $[Cp^*Rh(bpy)H]^+$, followed by the second tandem catalytic reaction to provide the biomimetic 1,4-NADH co-factor, **1**, for a hydride transfer to the Zn(II) bound carbonyl group of 2-pentanone, followed by a protonation of the Zn(II)-*S*-2-pentoxy bond to provide *S*-2-pentanol.

catalysis explored in the present investigation are provided in Table 1.

Molecular Dynamics Simulations of the Ternary Complex in Solution

Classical molecular dynamics (MD) simulations were initially performed to characterize the structure and dynamics of the HLADH-ketone-N-benzyl-1,4-dihydronicotinamide ternary complex, corresponding to the resting state of the enzyme catalysis, in both the canonical and alternative mechanistic hypotheses. In this complex, the substrate, 2-pentanone, was coordinated to the Zn (II) center with a pro-*S* orientation. Therefore, only the *S*-enantiomer has been considered in this study, according to the experimental data reported by Fish et al.[24a], which clearly showed that the synthesis of chiral alcohols from 2-pentanone, catalyzed by HLADH in the presence of biomimetic co-factor, **1**, resulted in an enantiomeric excess of approximately 85% for the *S*-enantiomer, and much higher for phenyl substituted ketones, ~96–99% *S*-enantiomer.[24a]

The multiscale approach used in this study can be summarized as follows. Firstly, the conformational ensemble of the protein-ligand system was explored by conducting molecular dynamics (MD), to sample representative geometries from the respective MD trajectories . The extracted structures were then used as starting points for the potential energy surface (PES) scan performed with the ONIOM[29] method, in which the investigated reaction coordinate was gradually varied, by accounting for both the solvent and protein environment effect on the reaction center.For each point in the PES scan, the geometry of the reaction center (the QM region) was extracted, and its single point energy calculated in the vacuum using a DFT method. It is worth noting that no optimization was performed in the vacuum, while the reaction center's structure was kept "as it is" from the scan to guarantee that the scanned geometries of the reaction center remained consistent with those obtained within the protein core. For selected reaction paths, the DFT energies and dipoles calculated in the vacuum were employed to apply the MD-PMM[27,28] method, which allowed the calculation of the corresponding Gibbs Free Energy profiles. Further details on these procedures have been provided in the Methods Section.

The initial configuration of the MD simulation was constructed starting from the crystal structure of the ternary complex formed by 4-methylbenzyl alcohol and the natural 1,4-NADH co-factor, as described in the Methods Section. One 50 ns-long MD simulation was performed considering His51 in the singly protonated state on the ε-nitrogen atom; we named this trajectory as HIE51. A representative structure of the catalytic site in the HIE51 MD simulation is shown in Figure 2. The protein structure remained stable along the MD simulation, as can be seen from the root-mean-square-deviation reported in the SI.

The free energy barrier of a given reaction model, was categorized by adopting the following strategy: (i) from the potential energy surface scans, a set of geometries along a given reaction path, was generated; (ii) their energies and dipoles were calculated in the gas phase to generate the "unperturbed" properties to be used as a basis set for PMM calculations; (iii) the reactant's highest energy point (HEP) and product geometries were chosen according to the gas-phase profile, and were used to calculate the corresponding free energy differences with the MD-PMM approach[27,28] (more details concerning this procedure are reported in the Methods Section). For the sake of major clarity, all the schemes, (i)–(iii), were applied to selected reaction models, based on the response of ONIOM scans' analysis (*vide infra*).

As a starting configuration for the ONIOM energy scans, a representative configuration was extracted from the HIE51 MD trajectory. This was selected to ensure that the crucial geometrical parameters for the hydride transfer step closely resemble those hypothesized for the natural 1,4-NADH reaction;[16,30,31] namely, the C4–H of the biomimetic 1,4-NADH

Table 1. The HLADH reactions are described and labeled, while the protonation of the His51 is stated. The starting structure for the study of reaction model I and V is reported in panel **a** of Figure 3, the starting structure of model II in panel **b** of Figure 3 and the starting structure of models III, IV and VI in panel **c** of Figure 3.

Reaction	Mechanism	Pathway		His51
I	canonical	nonsynchronous		neutral
II	canonical	nonsynchronous		cationic
III	canonical	nonsynchronous	$+H_2O$	cationic
IV	canonical	synchronous	$+H_2O$	cationic
V	alternative	nonsynchronous		neutral
VI	alternative	nonsynchronous	$+H_2O$	cationic

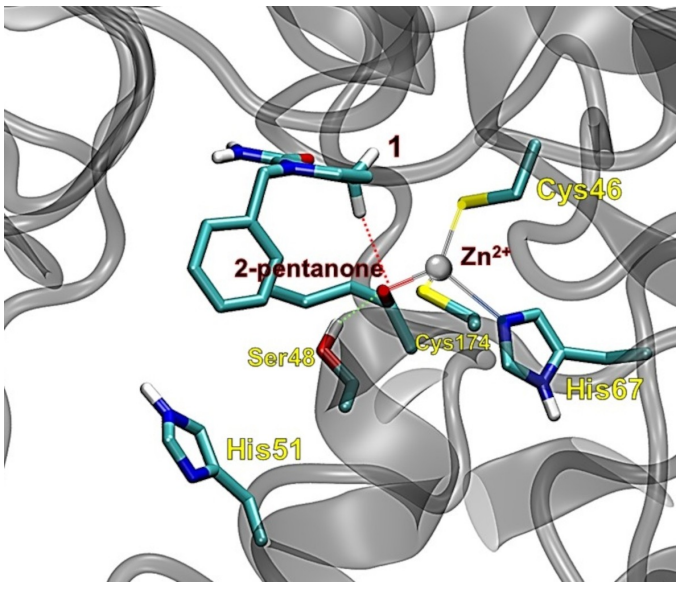

Figure 2. The reaction center of the enzyme, HLADH. In this figure, the coordination of the catalytic Zn(II) ion and relevant non-covalent contacts are rendered with bicolor and dashed lines, respectively. In this simulation, His51 is singly protonated on the ε-nitrogen atom.

co-factor, **1**, to the carbonyl acceptor, the C=O of 2-pentanone, with a distance of approximately of 4 Å, and a C4–Ĥ–C=O) angle close to 180°. The ONIOM calculations were performed through a QM/MM scheme, in which the quantum reaction center was chosen to include Cys46, Cys174, His67, His51, Zn(II), 2-pentanone, the substrate, co-factor **1**, and a water molecule when specified. Starting from this structure, three different initial configurations for the QM/MM energy scans were constructed and optimized at the QM/MM level using ONIOM (Figure 3). Moreover, we initially analyzed the reaction barrier involved in the canonical mechanism, which entailed a direct HT step from the biomimetic 1,4-NADH, **1**, to the substrate (Scheme 1). Subsequently, we examined the reaction barrier associated with the alternative mechanism proposal by Marrone and Fish,[26] and depicted in Scheme 2.

Models I and V were investigated starting from the configuration, in which His51 was neutral, and mono-protonated at the ε-N position; **structure a** in Figure 3. Models II and III were investigated starting from the configuration, in which His51 was cationic and doubly protonated, with either none (II), or one bridging water molecule (III); **structures b** and **c** in Figure 3. From each of these configurations, an energy scan was performed choosing the distance between the carbon of the ketone group, C=O, and the incipient hydride, H^-, as the reaction coordinate. This distance was varied from the initial value obtained after the QM/MM minimization; (see the caption for Figure 3) to 1.10 Å, the ideal C->H bond distance to the carbon atom of the C=>O group of 2-pentanone to form the *S*-2-pentoxy anion bound to Zn(II).

For each step of the ONIOM scan, the geometry of the QM region was extracted, with the Cα atoms saturated with hydrogen atoms, and the energy calculated in vacuum through a single point gas-phase calculation. This methodology guaranteed that the geometries remained consistent with those obtained within the protein. The energy barrier along each of the four profiles is shown in Figure 4. The lowest barrier was found in the reaction model I, with the HIE51 in the quantum center, and in the absence of a bridging water molecule.

The same procedure was applied to the study of the alternative mechanism by the way of reaction models, V–VI. As reported in Scheme 2, this mechanism was composed of two different phases; initially, His67 was released from the catalytic Zn(II) ion, leading to the η^2-5,6 C=C bond coordination of the biomimetic co-factor, **1**, to the Zn(II) metal ion center. This step was followed by the hydride transfer from biomimetic co-factor **1** to the C=O of 2-pentanone. For the η^2 complex formation step, the length of the Zn-δN coordinative bond was varied in 40 steps from 2.38 to 4.00 Å, while the HT step was investigated utilizing the same reaction coordinate used in the case of the canonical mechanism. The results of the ONIOM scans, followed by the gas-phase calculations, unequivocally indicated that the alternative mechanism was not viable, since the total energy barrier calculated for the reaction models, V–VI, was always higher than 35 kcal/mol, and independent of the protonation state of the His51, or either in the presence or absence of a bridging water molecule (see Figure 4). The His67 release process was largely endothermic, and was followed by a substantial energy barrier, in the 25–30 kcal/mol range, for the subsequent hydride transfer from the η^2-Zn (II) complex of co-factor **1**, to the C=O of 2-pentanone.

By utilizing this basis data, we proceeded with the free energy calculations just for the reaction model I, featured by the lowest gas-phase energy barrier, and for the reaction model V, starting from the same ternary complex as the reaction model I, by employing the PMM approach; details on the PMM approach in the Methods Section and in previous work.[27,28] Considering that a crucial objective of this investigation was to ascertain the activation free energy of the hydride transfer

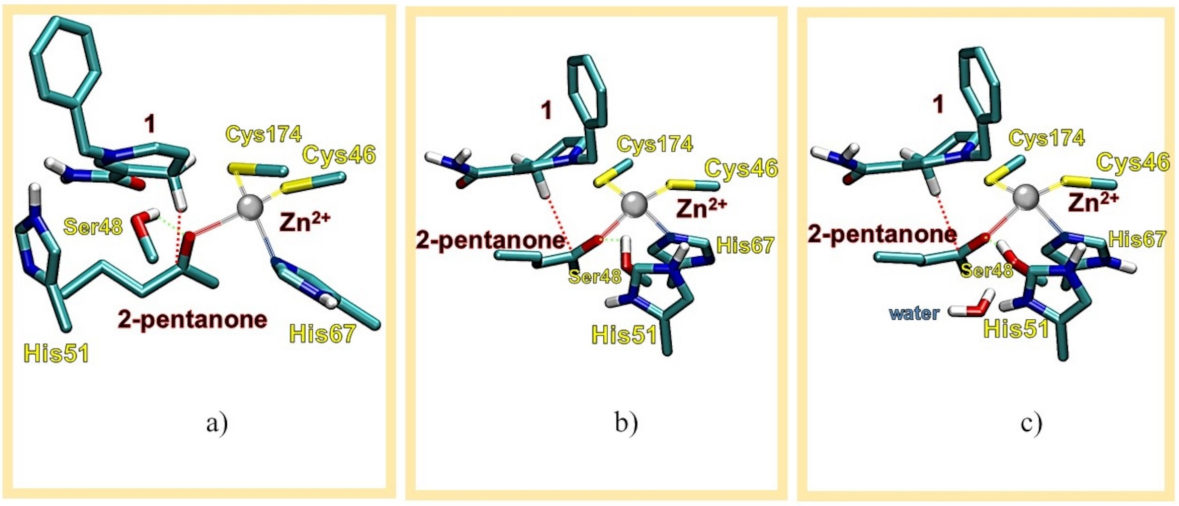

Figure 3. ONIOM-optimized structures of the first point used in the ONIOM scans. The reaction center, which was treated at the QM level in the ONIOM scans, is shown. All amino acids of the reaction center were truncated at the Cα in the QM/MM calculations. a) His51 was singly protonated on the ε-nitrogen; b) His51 was doubly protonated; and c) His51 was doubly protonated, and a water molecule was also inserted between His51 and Ser48. The H--C acceptor distance for each structure is highlighted in (**red**) (dashed lines); (a) 2.63 Å, (b) 2.59 Å, and (c) 2.52 Å, while the coordination of Zn(II) is highlighted with bicolor lines.

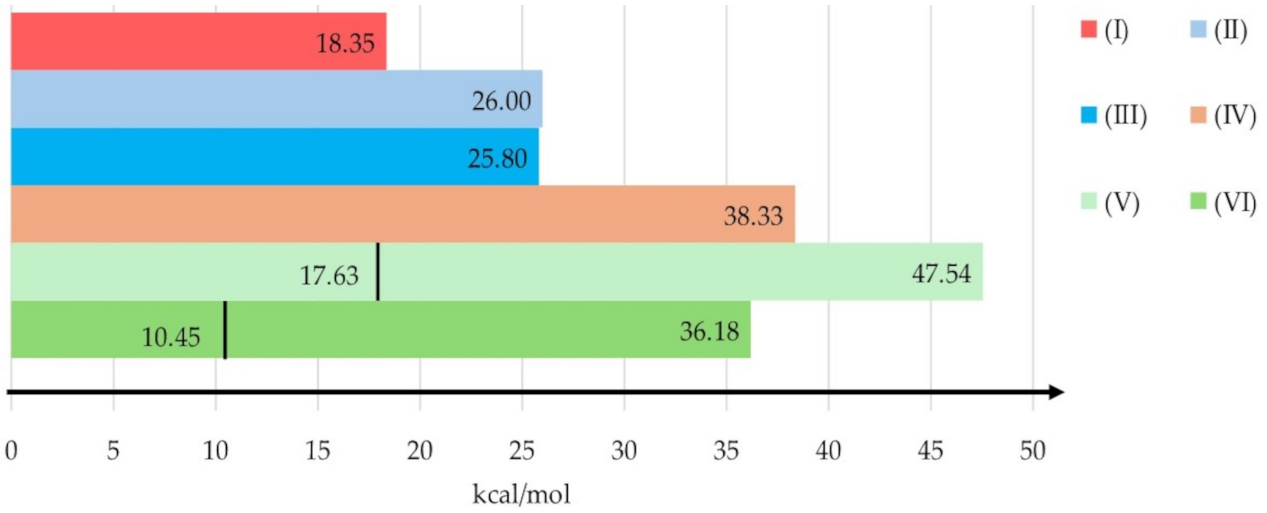

Figure 4. Gas-phase energy barrier along each mechanistic path. The **black** line in the alternative mechanisms V and VI indicated the value of the energy barrier for the His67 release step. The starting structure of the mechanisms I and V is reported in Figure 3a, and that for mechanism II in Figure 3b, and those for the mechanisms, III, IV, and VI, in Figure 3c.

reaction, we selected three points of the scan for reaction model I. This corresponded to the reactant (**first point**), the transition state-like structure (**the highest energy point**), and the product state (**last point**) of the hydride transfer step. Furthermore, four points of the scan for reaction model V; the reactant (**first point**), the 5,6-η^2-intermediate formed when the imidazole ligand was dissociated from Zn(II) (**point 29**), and the transition state-like structure for the hydride transfer step (**the highest energy point**), while also including the product state (**last point**).

The free energy values, and corresponding structures, gained by the PMM analysis for reaction model I are reported in Figure 5 (**left**). As shown, the late transition state-like structure provided further evidence of the important role played by the protein environment in favoring a close approach of the co-factor to the ketone carbonyl group. More importantly, from the PMM calculations, a free energy barrier, $\triangle G^{\#} = 13.8$ kcal/mol, was obtained. This value was in good agreement with the experimental value of 14 kcal/mol.[16] The distance between the hydride and the carbon atom at the highest energy point was 1.30 Å, and the C4–H–C=O angle was 153°. These geometrical parameters were in good agreement with previous calculations.[16,30,31]

The **Left** scheme encompassed three critical points; the reactant adduct (**RA**), the point of highest energy (**HEP**), which can be considered in close proximity to the transition state, and the product adduct (**PA**). The **Right** scheme encompassed four critical points; the reactant adduct (**RA**), the 5,6-η^2-complex formed in the imidazole dissociation from Zn(II), the point of highest energy (**HEP**), which can be considered in close proximity to the transition state, and the product adduct (**PA**). These structures are rendered by highlighting the interatomic distances of relevance in the modeled processes, such as the distance between the transferred hydride and the carbonyl carbon of 2-pentanone, which was treated as the reaction

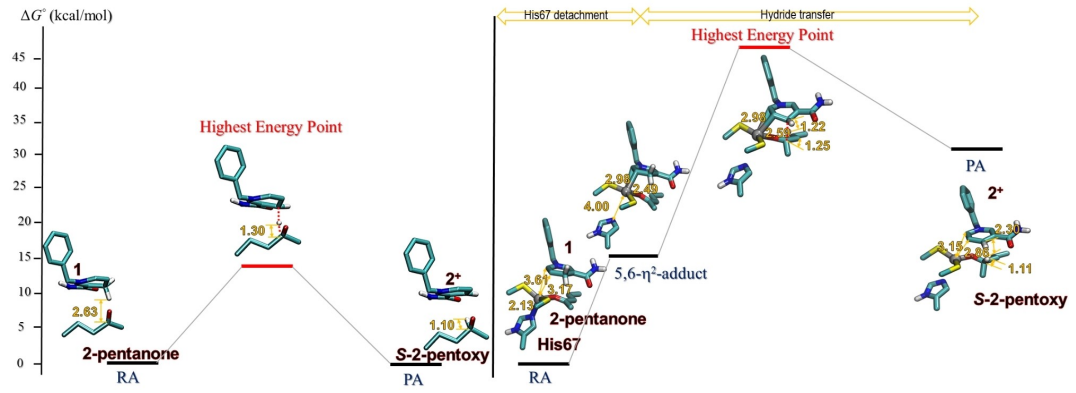

Figure 5. PMM reaction pathways are depicted, illustrating the Gibbs' free energy barrier of the reaction model I(**left**) and V(**right**). The error in the transition free energy $\Delta G^{\#}$ for the reaction model I and V is 1.8 and 2.4 kcal/mol, respectively, and is calculated as the mean (averaged over the two $\Delta G^{\#}$ values) standard error, obtained by dividing the productive MD trajectory into three sets.

coordinate, during the hydride transfer scans (All distance values in **Å**).

The PMM analysis of the reaction model V, yielding an overall free energy barrier of ~44 kcal/mol, and a barrier of ~28 kcal/mol for the **HT** step (Figure 5, **right**), corroborated the high endothermicity of this mechanistic hypothesis, demonstrated its mechanistic non-viability. Interestingly, in this case, the effect of the protein/solvent on the barrier was ~3–4 kcal/mol, consistent with what was found for the reaction model I.

The Proton Transfer Step, Following the Direct Hydride Transfer

We have focused on the proton transfer (**PT**) steps, following the direct **HT** for the canonical mechanism. Although the reaction models II and III were featured by a cationic His51 located to accomplish the proton relay, no evidence of a concomitant proton transfer was realized from the corresponding **HT** scans. It was generally believed that the proton transfer, affording the release of the chiral *S*-alcohol product, is sequential, and occurring after the hydride transfer step.However, Hammes-Schiffer et al. did not rule out the possibility that the **HT** and **PT** steps occurred in a concerted process,[16,30] thus, we decided to also test the viability of a concerted **HT+PT** mechanism, consistent with the reaction model IV (Table 1). In the calculations of both the sequential proton transfer step, reaction models II and III, and the concerted **HT+PT** step, reaction model IV, the His51 was then modeled in the doubly protonated state (HIP51), in agreement with the previous literature results.[16,30]

Starting from the product structure of the hydride transfer step, when the *S*-2-pentoxy anion was formed, an ONIOM scan was performed, moving only the proton of Ser48 closer to the oxygen of the *S*-2-pentoxy anion from a distance of 1.50 Å to a distance of 0.90 Å. This scan clearly showed that only by moving the hydrogen from Ser48 to the *S*-2-pentoxy anion, a proton transfer from His51 to Ser48, mediated by the water molecule, could occur spontaneously. The process, shown in Figure 6, was largely exothermic (~16 kcal/mol), with a small energy barrier of 1.30 kcal/mol, while the concerted mechanism displayed a total energy barrier of 38 kcal/mol.

To determine whether the bridging water molecules, between the doubly protonated His51 and Ser48 were important, an additional 50 ns-long MD simulation was performed considering His51 in its doubly protonated state, as a HIP51 trajectory. The HIP51 simulation displayed a single water molecule directly bridging the ε-N–H group of His51 and the OH group of Ser48, via a hydrogen bond, in 2.5% of the structures. In addition, 8% of the structures showed two, three or four bridging water molecules, creating a hydrogen bonding network between the ε-NH atom of His51, and the O atom of Ser48. According to previous studies,[14,16,30] the ribose group of the natural 1,4-NADH played a pivotal role in the proton transfer step; see the mechanism in Scheme 1.

The molecular mechanisms utilized with the biomimetic 1,4-NADH co-factors, including co-factor **1**, have somehow compensated for the absence of this functional group, and reasons why have remained elusive. The presence of one or more water molecules bridging Ser48 and cationic His51 through a hydrogen bond network, along our MD simulation, strongly suggested that when the natural 1,4-NADH co-factor was substituted with the simplified biomimetic 1,4-NADH co-factor, **1**, the reason for the function of the OH groups in position 2 and 3 of the ribose group, might have been critical for the role of one or more water molecules. Moreover, this group of water molecules could also potentially act as a "proton bridge" between His51 and Ser48 in the proton transfer, utilizing the biomimetic 1,4-NADH co-factor, **1**, as shown in Scheme 3.

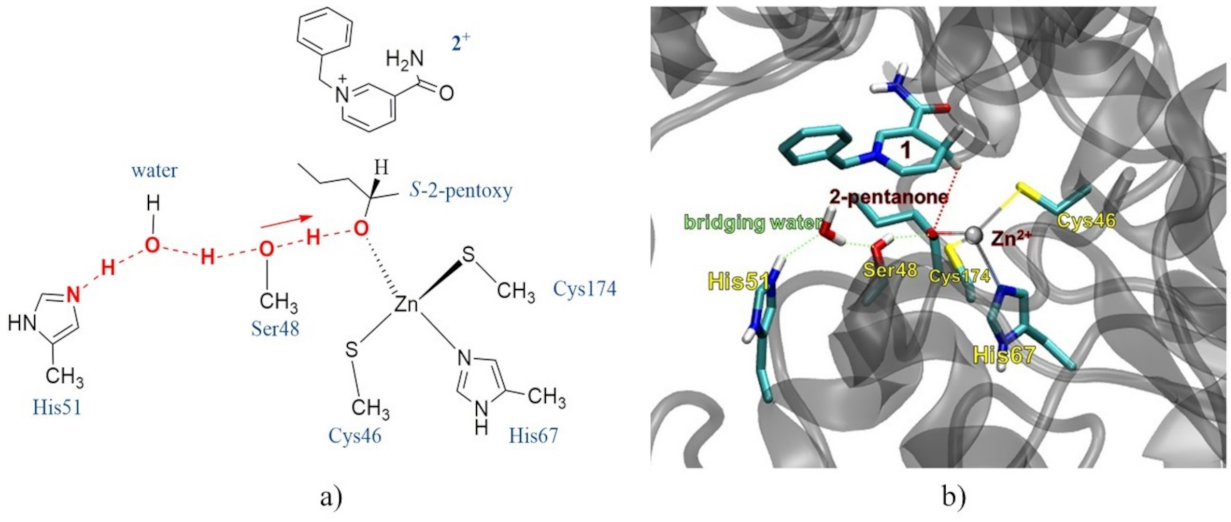

Figure 6. a) The proton transfer chain in the xTB scan, highlighted by the atoms and the dashed bonds in (**red**). The proton transfer path from His51 to the Zn(II) bound *S*-2-pentoxy anion in the xTB scan is triggered by moving the hydrogen atom on Ser48 toward the oxygen of the *S*-2-pentoxy anion ((red arrow)). **b**) Reaction center of HLADH in the configuration with the doubly protonated His51. In this structure, extracted from MD simulations, the presence of the bridging water between His51 and Ser48 are clearly visible; highlighted with dashed (**green lines**).

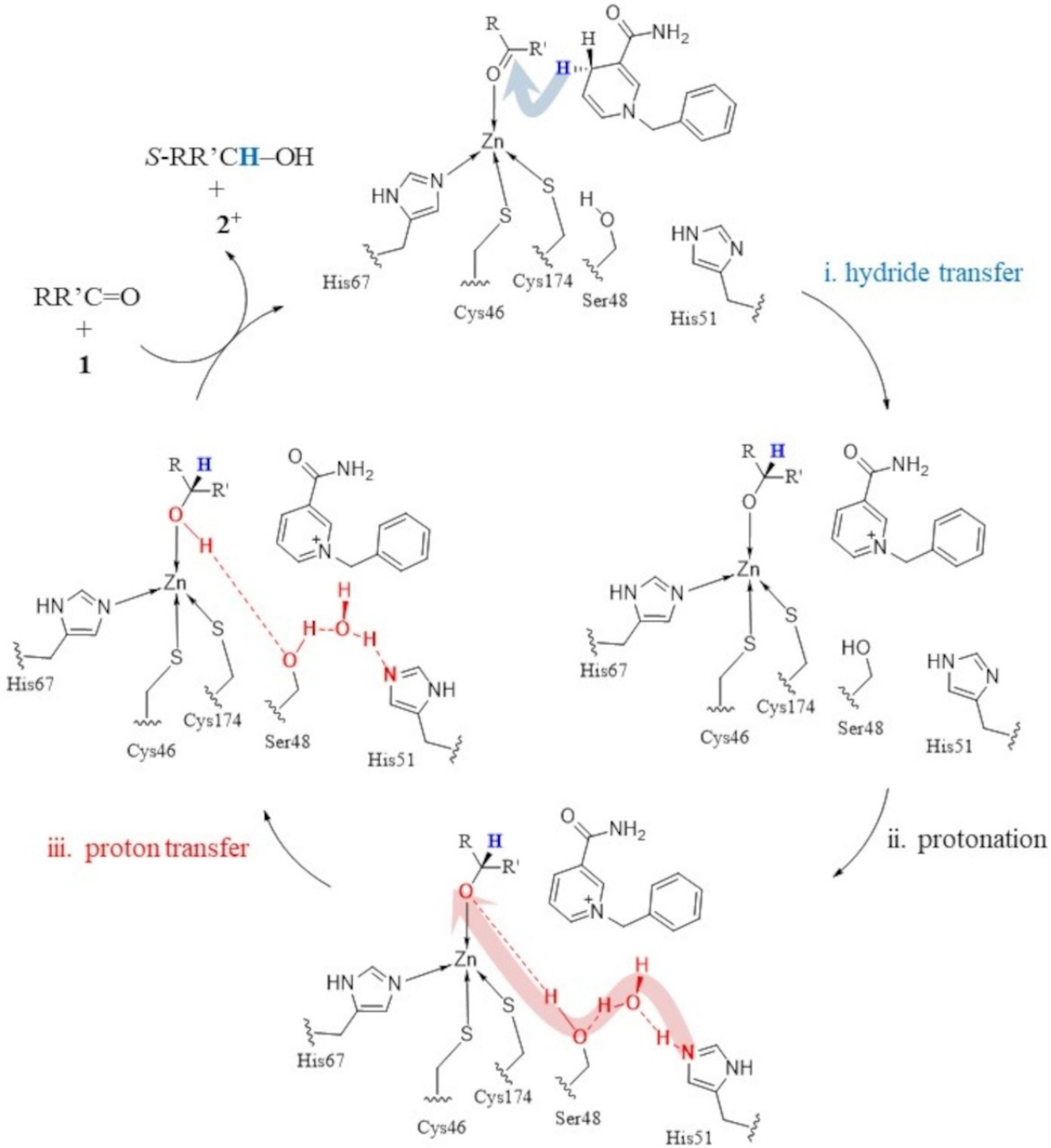

Scheme 3. HLADH-catalyzed reduction of a prochiral ketone substrate in the presence of the biomimetic co-factor, 1,4-NADH, **1**. The atoms involved in the proton relay and the hydride are colored, (**red**) and (**blue**), respectively.

Conclusions

In summary, our computational study has provided a detailed mechanistic insight of the HLADH enzyme catalysis, for the chiral reduction of prochiral ketones to chiral *S*-alcohols, in the presence of the 1,4-NADH biomimetic co-factor, **1**, as epitomized in Scheme 3. Calculations clearly showed that the alternative mechanism, in Scheme 2 proposed by Marrone and Fish,[26] in the absence of the proteins surrounding the HLADH active site for reactivity, was not viable, since the energy costs concerning the His decomplexation, and the subsequent **HT** transfer, provided an overall barrier higher than 35 kcal/mol. The HLADH catalysis in the presence of the biomimetic co-factor, **1**, occurred instead, via the canonical mechanism, with the initial step represented by a direct hydride transfer from the C4–H of biomimetic co-factor **1**, to the carbonyl C=O group of the substrate, 2-pentanone, to form the *S*-2-pentoxy anion, and then provided the chiral *S*-enantiomer for the product, *S*-2-

pentanol. Moreover, the lowest energy barrier for the **HT** was with the His51 in its neutral ionization state, thus suggesting that the His51 protonation may occur later, being consistent with the reaction model I (Table 1). Importantly, the estimated free energy barrier of about 14 kcal/mol for the **HT** step resulted in being in close agreement with the available experimental data.[16]

Following the **HT** step, a series of proton transfers ensued; the His51 imidazole was protonated by the bulk, and the proton was then relayed to the oxygen of Ser48, which further donated the proton to the substrate, the *S*-2-pentoxy anion. This process was mediated by one or two water molecules situated between His51 and Ser48 (Figure 6), and eventually with the formation of the *S*-2-pentanol, as the final step of the catalytic cycle. Therefore, the formation of a water bridge, connecting the protonated His51 and Ser48, and with a H-bond pattern consistent with the eventual Ser48 proton transfer to the Zn(II) bound *S*-2-pentoxy anion, resulting in an important protonation step, which was detected in about 11% of the MD trajectory. Moreover, the calculations of the energy profiles for the proton transfer through the water-mediated chain indicated that this process was very rapid, and occurred in an almost concerted step (Figure 5). The latter outcome also suggested that the HLADH catalysis, within the limits of the non-denaturating conditions, might be marginally influenced by the pH of the bulk medium. This result was in agreement with experimental evidence, which showed a relatively non-dependence of the HLADH catalysis on the bulk pH in the 6–10 range of values.[32]

These overall results have provided a Scheme 3 that verifies that the 1,4-NADH biomimetic, **1**, provided a different protonation mechanism, in comparison to the natural 1,4-NADH, for the critical proton transfer reaction of the water bridge, connecting the Ser48 proton transfer to the *S*-2-pentoxy anion bound to Zn(II), which led to the release of the chiral *S*-2-pentanol, while maintaining the exact *S*-enantiomer chirality afforded by the natural 1,4-NADH co-factor. This important HLADH enzyme computational mechanistic study could also create an economic benefit for the Biocatalysis Industry, since the utilization of the biomimetic co-factor, 1,4-NADH, **1**, and other likely derivatives of **1**, could reduce the synthesis cost of the production of chiral *S*-alcohols, and other enzyme products needing the natural 1,4-NADH co-factor, by a factor of ~16!

Computational Methods

Molecular Dynamics (MD) Simulations

The starting structure for the simulations at 300 K was taken from the refined crystal structure of the horse liver alcohol dehydrogenase (PDB entry 7 K35).[33] A molecule of 2-pentanone was added to the protein and aligned to the co-crystallized substrate i.e. 4-methylbenzyl alcohol. The same procedure was used to attach a N-Benzyl group to the 1,4-dihydronicotinamide nucleus, as the 1,4-NADH biomimetic co-factor. The protonation state of the His side chains was selected through the PropKa server.[34,35] For His51, two different charge states; namely, +0 with the proton on the ε-N (HIE51 trajectory), and +1 with both the δ-N and the ε-N protonated (HIP51 trajectory), were chosen and MD simulations were performed in both states. All simulations were performed with the GROMACS software.[36] The AMBER 99 force-field[37] was used for the protein and GAFF[38] for the organic molecules (2-pentanone and N-Benzyl-1,4-dihydronicotinamide,**1**). The active site was modeled using a "bonded approach" adapted from the work of Li et al.[39] according to which the Zn(II) ion was bonded to the two sulfur atoms of Cys46, the oxygen atom of the substrate and the ε-N atom of His67. The charge state for residues Cys46 and Cys 174 was set to −1 (CYM residue type), for residue His67 to 0 (HID residue type) and for the Zn(II) ion to +2. The protein, with the substrate and the co-factor, was placed in a periodic cubic box with side length equal to 13.63 nm and solvated in water using the TIP3P model.[40] An appropriate number of counterions were added to achieve charge neutrality of the entire system. The Particle Mesh Ewald (PME) method[41] was used for the long-range electrostatic interactions applying a 0.132 Fourier spacing,[42] and a real space cutoff of 1.1 nm. The Lennard-Jones potential was truncated at 1.1 nm. A time step of 0.001 ps was employed in conjunction with the LINCS algorithm,[43] to constrain bond lengths involving polar hydrogen atoms. In the following minimization, annealing, and equilibration steps, the heavy atoms of the protein were restrained to their initial positions using a force constant of 1000 kJ mol^{-1} nm^{-2}. After the energy minimization, the temperature was increased from 50 K–300 K in 100 ps and an equilibration MD simulation of 2 ns was carried on in the NPT (constant number of particles, pressure and temperature) ensemble using the canonical V-Rescale thermostat[44] (relaxation time constant of 0.002 ps, T = 300 K) and the Berendsen barostat[45] (relaxation time of 1 ps, compressibility of 4.5 10^{-5}, P = 1 bar). After these initial equilibration steps, the restraints on the heavy atoms of the protein were released and all atoms of the reaction center; i.e., the atoms belonging to Cys46, Ser48, His51, His67, Cys174, Zn(II), N-Benzyl-1,4-dihydronicotinamide,**1**, and 2-pentanone were restrained to the starting positions using a force constant of 1000 kJ mol^{-1} nm^{-2}, and a 15 ns-long MD simulation was run in the NPT ensemble, using the same setup of the previous equilibration step. This step was followed by two additional 2 ns-long MD trajectories, in which the force constant of the positional restraint was set to 100 kJ mol^{-1} nm^{-2} and 10 kJ mol^{-1} nm^{-2}, respectively. Finally, a 50 ns-long unrestrained MD simulation was carried on using a time step of 1 fs. This procedure was repeated for both protonation states of His51. Hydrogen bond networks that involve water molecules connecting His51 to Ser48 were investigated using an in-house tool. For defining hydrogen bonds, we have adopted the definition reported by Kumar et al.[46]

Quantum Mechanics/Molecular Mechanics (QM/MM) Calculations

All the structures of the HLADH, 2-pentanone, and the eN-Benzyl-1,4-dihydronicotinamide adduct, which were used in the QM/MM calculations were optimized with the ONIOM scheme implemented in the xTB program.[47] The high-level region, which included residues Cys46, Ser48, His51, His67 and Cys174, the 2-pentanone, the co-factor **1**, the catalytic Zn(II) ion, and water molecules, when specified, were treated at the GFN2-xTB,[48] while the rest of the protein was modeled with the GFN-FF force field level.[49]

The GFN2: GFN-FF geometry optimizations were carried out using the generalized Born solvation algorithm,[50] to simulate the aqueous environment, and with the fast inertial relaxation engine (FIRE),[51] with gradient and energy thresholds of 0.002 hartree/bohr and 0.00005 hartree, respectively. From each of the three starting geometries described in the main text (see Figure 3), we have computed the potential energy surface along reactions (I–VI) indicated in Table 1. The computation of the energy profiles were

accomplished using the same setup above, while also using a constrained optimization at each point. Apart from the distances involved in the reaction, no other constraints in the structure were imposed. Reaction IV was simulated using a concerted scan of two distances that were varied simultaneously to generate a 1-dimensional energy profile.

Perturbed Matrix Method (PMM)-MD Calculations

The basic features of the PMM-MD approach have been explained in detail in previous papers, and here only the essential aspects were mentioned.[52–54] The PMM-MD method was based on dividing the whole system into a quantum center (QC), where the quantum processes of interest occur, the hydride transfer reaction in the present case, treated at the electronic level, and the environment, modeled as an atomic-molecular semi-classical subsystem interacting with the QC.

In the present case, the QC chosen corresponded to the reaction center of the enzyme, which included residues Cys46, Ser48, His51, His67 and Cys174, the 2-pentanone, the co-factor **1**, the catalytic Zn(II) ion, and a water model when specified. The entire system, such as the QC, the remaining protein, and the solvent, were used to sample the phase space by means of MD simulation. The unperturbed electronic Hamiltonian (H^o) of the isolated QC was calculated at the B3LYP/6-31G* level of theory.[55–58] Thus, for each configuration of the entire system extracted from the MD simulation, the electrostatic perturbation of the external environment was evaluated on the QC center of mass, and used for constructing the perturbed electronic Hamiltonian matrix $\widehat{H}$ according to Equations (1–2):

$$\widehat{H} = \widehat{H}_0 + \widehat{I}\, q_T\, V + \widehat{Z}_1 \quad (1)$$

$$\widehat{Z}_1 = -\boldsymbol{E} \cdot \langle \phi_j^0 | \widehat{\boldsymbol{\mu}} \, | \phi_i^0 \rangle \quad (2)$$

Where $\widehat{H_0}$ was the unperturbed electronic Hamiltonian matrix, q_T was the total charge, $\widehat{\boldsymbol{\mu}}$ was the dipole operator, V and $\boldsymbol{E}$ were, respectively, the electrostatic potential and field exerted by the environment on the QC center of mass at each frame of the simulation, ϕ^0 are the unperturbed (gas-phase) electronic eigenstates of the QC, and $\widehat{I}$ was the identity matrix.

The diagonalization of the matrix (1) at each MD frame provided a set of eigenvalues and eigenvectors. Furthermore, the QC properties/observables of interest can be calculated as a function of time; for example, the perturbed energy in the present case. In the case of the Gibbs' free energy difference ($\triangle G^0$), this quantity was calculated according to Equation (3):

$$\Delta G^0 \simeq -k_b T \ln \left[\frac{1}{N} \sum_{i=1}^{N} \exp\left(-\frac{\Delta E_i}{k_b T} \right) \right] \quad (3)$$

Thus, k_b was the Boltzmann constant, N was the number of frames of the MD trajectory, and $\triangle E_i$ was the QC perturbed electronic energy difference between two points. All quantities, E and G, were calculated in the *NPT* ensemble, $T = 300$ K, and $P = 1$ bar, were the conditions used in the MD simulation. In the present case, $\triangle G^\circ$ values were evaluated for the highest energy point, and for the product relative to the reactant. Note also that in this equation, we have neglected the contribution to the free-energy, due to the vibrational energy shifts between the two points.

Acknowledgements

We acknowledge the CINECA award under the ISCRA initiative, for the availability of high performance computing resources and support. The original synthesis and utilization of the biomimetic co-factor, **1**, in the biocatalysis studies, were supported by US Department of Energy funding from the Advanced Energy Projects and Technology Research Division, Office of Computational and Technology Research (RHF), under Contract No. DE ACO2-05CH11231 Open Access publishing facilitated by Università degli Studi Gabriele d'Annunzio Chieti Pescara, as part of the Wiley - CRUI-CARE agreement.

Conflict of Interests

The authors declare no competing interests.

Data Availability Statement

The data that support the findings of this study are available from the corresponding author upon reasonable request.

Keywords: Biocatalysis · Enantioselectivity · Oxidoreductase · Co-factors · Molecular dynamics · Density functional calculations

[1] E. L. Bell, W. Finnigan, S. P. France, A. P. Green, M. A. Hayes, L. J. Hepworth, S. L. Lovelock, H. Niikura, S. Osuna, E. Romero, K. S. Ryan, N. J. Turner, S. L. Flitsch, *Nat. Rev. Methods Prim.* **2021**, *1*, 1–21.
[2] R. T. Kumar, R. Sreedharan, P. Ghosh, T. Gandhi, D. Maiti, *Chem.-A Eur. J.* **2022**, *28*, e202103949.
[3] R. Buller, S. Lutz, R. J. Kazlauskas, R. Snajdrova, J. C. Moore, U. T. Bornscheuer, *Science* **2023**, *382*, 8615.
[4] R. Callender, R. B. Dyer, *Acc. Chem. Res.* **2015**, *48*, 407–413.
[5] X. Sheng, M. Kazemi, F. Planas, F. Himo, *ACS Catal.* **2020**, *10*, 6430–6449.
[6] Y. Wu, W. Xu, L. Jiao, W. Gu, D. Du, L. Hu, Y. Lin, C. Zhu, *Chem. Soc. Rev.* **2022**, *51*, 6948–6964.
[7] A. R. Alcántara, P. Domínguez de María, J. A. Littlechild, M. Schürmann, R. A. Sheldon, R. Wohlgemuth, *ChemSusChem* **2022**, *15*, e202102709.
[8] R. Agudo, G. D. Roiban, M. T. Reetz, *J. Am. Chem. Soc.* **2013**, *135*, 1665–1668.
[9] I. Victorino da Silva Amatto, N. Gonsales da Rosa-Garzon, F. Antônio de Oliveira Simões, F. Santiago, N. Pereira da Silva Leite, J. Raspante Martins, H. Cabral, *Biotechnol. Appl. Biochem.* **2022**, *69*, 389–409.
[10] S. B. J. Kan, R. D. Lewis, K. Chen, F. H. Arnold, *Science* **2016**, *354*, 1048–1051.
[11] R. S. Molina, G. Rix, A. A. Mengiste, B. Álvarez, D. H. Seo, H. Chen, J. E. Hurtado, Q. Zhang, J. D. García-García, Z. J. Heins, P. J. Almhjell, F. H. Arnold, A. S. Khalil, A. D. Hanson, J. E. Dueber, D. V. Schaffer, F. Chen, S. Kim, L. Á. Fernández, M. D. Shoulders, C. C. Liu, *Nat. Rev. Methods Prim.* **2022**, *2*, DOI: 10.1038/s43586-022-00119-5.
[12] A. G. McDonald, K. F. Tipton, *FEBS J.* **2023**, *290*, 2214–2231.
[13] A. Marrone, R. H. Fish, *Organometallics* **2023**, *42*, 288–306.
[14] B. V. Plapp, *Arch. Biochem. Biophys.* **2010**, *493*, 3–12.
[15] S. Ramaswamy, H. Eklund, B. V. Plapp, *Biochemistry* **1994**, *33*, 5230–5237.
[16] K. Agarwal, S. P. Webb, S. Hammes-Schiffer, *J. Am. Chem. Soc.* **2000**, *122*, 4803–4812.
[17] B. J. Bahnson, T. D. Colby, J. K. Chin, B. M. Goldstein, J. P. Klinman, *Proc. Natl. Acad. Sci. U. S. A.* **1997**, *94*, 12797–12802.
[18] H. C. Lo, J. D. Ryan, J. B. Kerr, D. S. Clark, R. H. Fish, *J. Organomet. Chem.* **2017**, *839*, 38–52.
[19] R. H. Fish, *Catalysts* **2019**, *9*, 562.
[20] D. P. Smith, E. Baralt, B. Morales, M. M. Olmstead, M. F. Maestre, R. H. Fish, *J. Am. Chem. Soc.* **1992**, *9*, 10647–10649.

[21] H. Eklund, S. Ramaswamy, *Cell. Mol. Life Sci.* **2008**, *65*, 3907–3917.
[22] J. R. Sunderland, X. E. E. TaoButrick, E. E. Butrick, L. C. Keilich, C. E. Villa, J. R. Miecznikowski, S. S. Jain, *Polyhedron* **2016**, *114*, 145–151.
[23] R. H. Fish, *Advances in Bioorganometallic Chemistry: Organometallic Chemistry at the Interface with Biology* (Eds: T. Hirao, T. Moriuchi), Elsevier, Amsterdam, The Netherlands, **2019**, Ch. 1, 3–33.
[24] a) H. C. Lo, R. H. Fish, *Angew. Chem. Int. Ed. Engl.* **2002**, *41*, 478; b) Y. H. Fu, G. Bin Shen, K. Wang, X. Q. Zhu, *ChemistrySelect* **2021**, *6*, 80078010
[25] T. Knaus, C. E. Paul, C. W. Levy, S. De Vries, F. G. Mutti, F. Hollmann, N. S. Scrutton, *J. Am. Chem. Soc.* **2016**, *138*, 1033–1039.
[26] A. Marrone, R. H. Fish, *J. Organomet. Chem.* **2021**, *943*, 121810.
[27] O. Zanetti-Polzi, L. M. Aschi, A. Amadei, I. Daidone, *J. Phys. Chem. Lett.* **2017**, *8*(14), 3321–3327.
[28] A. Amadei, I. Daidone, M. Aschi, *Phys. Chem. Chem. Phys.* **2012**, *14*, 1360–1370.
[29] L. W. Chung, W. M. C. Sameera, R. Ramozzi, A. J. Page, M. Hatanaka, G. P. Petrova, T. V. Harris, X. Li, Z. Ke, F. Liu, H. B. Li, L. Ding, K. Morokuma, *Chem. Rev.* **2015**, *115*, 5678–5796.
[30] Q. Cui, M. Elstner, M. Karplus, *J. Phys. Chem. B* **2002**, *106*, 2721–2740.
[31] S. P. Webb, P. K. Agarwal, S. Hammes-Schiffer, *J. Phys. Chem. B* **2000**, *104*, 8884–8894.
[32] R. L. Brooks, J. D. Shore, H. Gutfreund, *J. Bio. Chem.* **1972**, *247*, 2382–2383.
[33] B. V. Plapp, R. Subramanian, *Arch. Biochem. Biophys.* **2021**, *701*, 108825.
[34] M. H. M. Olsson, C. R. Søndergaard, M. Rostkowski, J. H. Jensen, *J. Chem. Theory Comput.* **2011**, *7*, 525–537.
[35] C. R. Søndergaard, M. H. M. Olsson, M. Rostkowski, J. H. Jensen, *J. Chem. Theory Comput.* **2011**, *7*, 2284–2295.
[36] M. J. Abraham, T. Murtola, R. Schulz, S. Páll, J. C. Smith, B. Hess, E. Lindahl, *SoftwareX* **2015**, *1–2*, 19–25.
[37] V. Hornak, R. Abel, A. Okur, B. Strockbine, A. Roitberg, C. Simmerling, *Proteins: Struct., Funct., Bioinf.* **2006**, *65*, 712–725.
[38] J. Wang, R. M. Wolf, J. W. Caldwell, P. A. Kollman, D. A. Case, *J. Comput. Chem.* **2004**, *25*, 1157–1174.
[39] F. Lin, R. Wang, *J. Chem. Theo. Comp.* **2010**, *6*(6), 1852–1870.
[40] W. L. Jorgensen, J. Chandrasekhar, J. D. Madura, R. W. Impey, M. L. Klein, *J. Chem. Phys.* **1983**, *79*, 926–935.
[41] T. Darden, D. York, L. Pedersen, *J. Chem. Phys.* **1993**, *98*, 10089–10092.
[42] E. O. Brigham, R. E. Morrow, *IEEE Spectr* **1967**, *4*, 63–70.
[43] B. Hess, H. Bekker, H. J. C. Berendsen, J. G. E. M. Fraaije, *J. Comput. Chem.* **1997**, *18*, 1463–1472.
[44] G. Bussi, D. Donadio, M. Parrinello, *J. Chem. Phys.* **2007**, *126*, 014101.
[45] H. J. C. Berendsen, J. P. M. Postma, W. F. van Gunsteren, A. DiNola, J. R. Haak, *J. Chem. Phys.* **1984**, *81*, 3684–3690.
[46] R. Kumar, J. R. Schmidt, J. L. Skinner, *J. Chem. Phys.* **2007**, *126*, 204107.
[47] C. Bannwarth, E. Caldeweyher, S. Ehlert, A. Hansen, P. Pracht, J. Seibert, S. Spicher, S. Grimme, *WIREs Comput. Mol. Sci.* **2021**, *11*, e1493.
[48] C. Bannwarth, S. Ehlert, S. Grimme, *J. Chem. Theory Comput.* **2019**, *15*(3), 1652–1671.
[49] S. Spicher, S. Grimme, *Angew. Chem. Int. Ed.* **2020**, *59*(36), 15665–15673.
[50] A. V. Onufriev, D. A. Case, *Annu. Rev. Biophys.* **2019**, *48*(1), 275–296.
[51] J. Guenole, W. G. Nöhring, A. Vaid, F. Houlle, Z. Xie, A. Prakash, E. Bitzek, *Comput. Mater. Sci.* **2020**, *175*, 109584.
[52] L. Zanetti-Polzi, M. Aschi, A. Amadei, I. Daidone, *J. Phys. Chem. Lett.* **2017**, *8*(14), 3321–3327.
[53] M. Aschi, V. Barone, B. Carlotti, I. Daidone, F. Elisei, A. Amadei, *Phys. Chem. Chem. Phys.* **2016**, *18*, 28919–28931.
[54] L. Zanetti-Polzi, A. Amadei, R. Djemili, S. Durot, L. Schoepff, V. Heitz, B. Ventura, I. Daidone, *J. Phys. Chem. C.* **2019**, *123*(20), 13094–13103.
[55] D. Becke, *J. Chem. Phys.* **1993**, *98*, 5648–5652.
[56] T. Clark, J. Chandrasekhar, G. W. Spitznagel, P. V. R. Schleyer, *J. Comput. Chem.* **1983**, *4*(3), 294–301.
[57] P. C. Hariharan, J. A. Pople, *Theo. Chim. Acta* **1973**, *28*(3), 213–222.
[58] W. J. Hehre, R. Ditchfield, J. A. Pople, *J. Chem. Phys.* **1972**, *56*(5), 2257–2261.

Manuscript received: September 19, 2024
Accepted manuscript online: September 25, 2024
Version of record online: ■■, ■■

RESEARCH ARTICLE

The HLADH catalysis of the *S*-enantioselective reduction of 2-pentanone, operating in presence of the biomimetic co-factor, N-benzyl-1,4-dihydronicotinamide, **1**, occurred via the direct hydride transfer to form the *S*-2-pentoxy anion, followed by a water bridge, connecting the Ser48 proton relay to the final release step of the chiral *S*-2-pentanol.

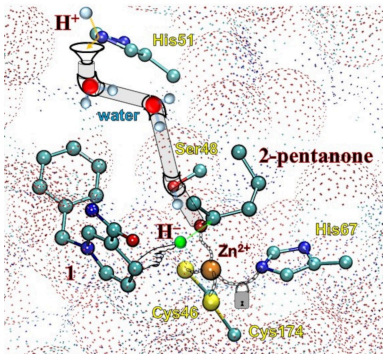

M. Farina, M. Capone, E. Bodo, R. H. Fish, M. Aschi, A. Marrone*, I. Daidone**